Optics Communications 428 (2018) 41–46

Contents lists available at ScienceDirect

Optics Communications

journal homepage: www.elsevier.com/locate/optcom

Performance-improved microwave photonic single-passband filter using birefringence of phase-shifted fiber Bragg grating

Enming Xu [a], Shilong Pan [b,*], Zuxing Zhang [a], Peili Li [a]

[a] Advanced Photonic Technology Laboratory, Nanjing University of Posts and Telecommunications, Nanjing 210023, China
[b] Key Laboratory of Radar Imaging and Microwave Photonics, Ministry of Education, Nanjing University of Aeronautics and Astronautics, Nanjing 210016, China

ARTICLE INFO

Keywords:
Microwave photonic
Microwave filter
Phase-shifted fiber Bragg grating

ABSTRACT

A novel microwave photonic single-passband filter with an improved out-of-band rejection and an extended frequency tuning range is proposed and demonstrated, which is achieved by using birefringence of a phase-shifted fiber Bragg grating (PSFBG). If two polarization states of two phase-modulated signals with opposite modulation indices from a polarization modulator (PolM) are controlled to be aligned with two principal axes of the polarization-maintaining PSFBG (PM-PSFBG), respectively, two single-passband or two single-notch filters with slight frequency interval are achieved, depending on the position of the optical carrier relative to the notches of the PM-PSFBG. Through subtraction of the two filters, the out-of-band rejection is significantly improved, and the frequency tuning range is greatly extended. Analytical simulations are performed using an established theoretical model, which are verified by an experiment.

1. Introduction

Over the past few decades, microwave photonic filters have been widely investigated thanks to broad bandwidth, insensitivity to electromagnetic interference, flexible tunability, and reconfigurability [1–4]. Of the filters, the highly required is a single-passband filter since it can overcome the limitation of a periodic frequency response implemented by a delay-line-based filter [5,6]. A variety of approaches have been proposed for implementing single-passband filters [7–22]. The approaches can be mainly classified into two categories. One is based on a sliced [7–9] or non-sliced [10–12] broadband source in combination with a dispersive element. The limitation for this category is that the broadband source is usually a non-communicational source and the dispersive component is usually a kilometers long optical fiber. The other is based on phase modulation to intensity modulation conversion [13–22]. The conversion can be achieved by many techniques. One technique is the use of stimulated Brillouin scattering; however, it is complicated because a pump source and a dispersive component are required [13,14]. Another technique is based on a semiconductor device, such as Fabry–Pérot semiconductor optical amplifier (FP-SOA) [15], distributed-feedback SOA (DFB-SOA) [16], or FP laser diode (FP-LD) [17]. However, due to the use of the active component, the filter has a poor stability and low out-of-rejection ratio. Although the out-of-band rejection ratio could be improved with the assistance of one more optical source [18], the cost and complexity are increased. Recently, using a phase-shifted FBG (PSFBG) [19–21] to realize a single-passband filter has drawn an attractive attention thanks to the simple structure. However, the performances, especially the out-of-band rejection and the frequency tuning range, are restricted by the current conventional approach, and can be improved further.

In this work, a single-passband filter based on a PSFBG with small birefringence is proposed. The PSFBG with small birefringence here is also called polarization maintaining PSFBG (PM-PSFBG). Adjusting the polarization state of a light wave to be oriented 45° relative to one principal axis of a PolM, two phase-modulated signals with opposite phase modulation indices along the two orthogonal principal axes are generated. Then the two polarization states of the phase-modulated signals are controlled to be aligned with two orthogonal principal axes of the PM-PSFBG, respectively. After reflection from the PM-PSFBG, two single-passband filters or two single-notch filters with slight frequency interval are realized, depending on the position of the optical carrier relative to the notches of the PM-PSFBG. Since the two filters are out of phase by 180°, the subtraction is performed between either the two single-passband filters or two single-notch filters. Thus, the out-of-band rejection is improved and the frequency tuning range is extended, compared to the conventional filter based on a common phase modulator (PM) and a common PSFBG [19–21]. A theoretical analysis

* Corresponding author.
E-mail address: pans@ieee.org (S. Pan).

https://doi.org/10.1016/j.optcom.2018.07.041
Received 2 May 2018; Received in revised form 11 July 2018; Accepted 12 July 2018
Available online 17 July 2018
0030-4018/

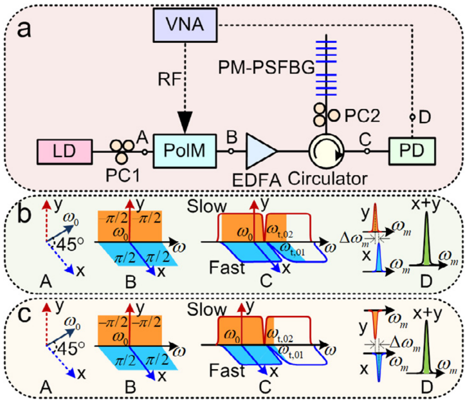

Fig. 1. (a) Block diagram of the proposed single-passband filter; the operation principle for achieving the improved filter through the subtraction of (b) two single-passband filters; (c) two single-notch filters. LD, laser diode; PC, polarization controller; PolM, polarization modulator; EDFA, erbium-doped fiber amplifier; PM-PSFBG, polarization maintaining phase-shifted fiber Bragg grating; PD, photodetector; VNA, vector network analyzer; RF, radio-frequency.

is performed, which is verified by an experiment. The simulated results are in good agreed with the experimental results.

2. Operational principle and theoretical analysis

The configuration and the operation principle of the proposed single-passband filter are depicted in Fig. 1. The proposed filter is composed of a laser diode (LD), a polarization controller (PC1), a PolM, an erbium-doped fiber amplifier (EDFA), a circulator, PC2, a PM-PSFBG with small birefringence and a photodetector (PD). The polarization state of the light wave from the LD is oriented 45° by PC1 with respect to one principal axis of the PolM, driven by a sweeping radio-frequency (RF) signal from a vector network analyzer (VNA), and two phase-modulated signals with opposite phase modulation indices along two principle axes (i.e. x, y) are generated. The modulated signals are amplified in the EDFA and subsequently input to the PM-PSFBG via a circulator, whose orthogonal polarization states are controlled by a second PC (PC2) to be aligned with the fast and slow axes of the PM-PSFBG, respectively. Thanks to the small birefringence existing in the PM-PSFBG, two ultra-narrow notches locating at $\omega_{t,01}$ (fast) and $\omega_{t,02}$ (slow) with slight spectral interval in reflection spectrum are obtained [23]. After reflection from the PM-PSFBG, the conversion from phase modulation to intensity modulation is achieved. Upon photodetection, two conventional single-passband filters or two single-notch filters with slight frequency interval are obtained, which depends on the position of the optical carrier relative to the notches of the PM-PSFBG, as shown in Fig. 1(b) and (c). The frequency interval between the two filters is determined by the spectral interval between the two notches of the PM-PSFBG. Since the phase modulation indices along the two principle axes of the PolM are opposite, and the two notches of the PM-PSFBG are located at the same side of the optical carrier, the realized two filters have a phase difference of 180°. Thus, subtraction between the two filters is performed, through subtraction, the out-of-band rejection is improved, and the frequency tuning range is extended.

Assuming a RF signal denoted as $\cos\omega_m t$ is applied to the PolM, and the polarization state of a light wave is oriented 45° relative to one principal axis of the PolM, the generated two complimentary phase-modulated signals are given by [22]

$$E_{x,y} = E_{in}\exp(\pm j\beta\cos(\omega_m t + \varphi_m)) \tag{1}$$

where $E_{in} = E_0\exp(j\omega_0 t)$, E_0 and ω_0 are the optical field and angular frequency of the LD, respectively; β is the phase modulation index, ω_m and φ_m represent the angular frequency and initial phase of the RF signal, respectively.

With the two polarization states of the two phase-modulated signals aligned with the fast and slow axes of the PM-PSFBG, after reflection, the expansion of the modulated signals under small signal modulation can be written as [20]

$$E_{x,y} = E_{in}\left(\begin{array}{l}\sqrt{r_{01,02}(\omega_0)}J_0(\beta)\exp\left(j\theta_{01,02}(\omega_0)\right)\\ +\sqrt{r_{01,02}(\omega_0+\omega_m)}J_1(\beta)\exp\left[j(\omega_m t+\varphi_m\pm\frac{\pi}{2})\right.\\ \left.+\,j\theta_{01,02}(\omega_0+\omega_m)\right]\\ +\sqrt{r_{01,02}(\omega_0-\omega_m)}J_1(\beta)\exp\left[-j(\omega_m t+\varphi_m\mp\frac{\pi}{2})\right.\\ \left.+\,j\theta_{01,02}(\omega_0-\omega_m)\right]\end{array}\right) \tag{2}$$

where $J_n(\cdot)$ with $n = 0$, 1 are the first kind Bessel functions, r_i and θ_i with $i = 01, 02$ represent, respectively, the reflective coefficient and phase response of the PM-PSFBG [20], which can be obtained using transmission-matrix approach [24], and the subscripts of $i = 01, 02$ denote the fast and slow axes, respectively. As seen from Eq. (2), both the amplitude and the phase of the optical carrier, as well as the sidebands, are changed by the PM-PSFBG, thus achieving phase modulation to intensity modulation conversion.

The overall power of the microwave signals can be expressed by

$$\begin{aligned}P(\omega_m) \propto{}& V_x^2 + V_y^2 - 2A_xA_y\\ &\times\left\{\begin{array}{l}\sqrt{r_{01}(\omega_0+\omega_m)}\left[\sqrt{r_{02}(\omega_0+\omega_m)}\cos(\theta'_{01}-\theta'_{02})\right.\\ \left.-\sqrt{r_{02}(\omega_0-\omega_m)}\cos(\theta'_{01}-\theta''_{02})\right]\\ -\sqrt{r_{01}(\omega_0-\omega_m)}\left[\sqrt{r_{02}(\omega_0+\omega_m)}\cos(\theta''_{01}-\theta'_{02})\right.\\ \left.-\sqrt{r_{02}(\omega_0-\omega_m)}\cos\left(\theta''_{01}-\theta''_{02}\right)\right]\end{array}\right\}\end{aligned} \tag{3}$$

In the above equation, the corresponding parameters are

$$\begin{aligned}V_{x,y}^2 ={}& A_{x,y}^2\cdot\left[r_{01,02}(\omega_0+\omega_m)+r_{01,02}(\omega_0-\omega_m)\right.\\ &\left.-\,2\sqrt{r_{01,02}(\omega_0+\omega_m)}\sqrt{r_{01,02}(\omega_0-\omega_m)}\cdot\cos(\theta'_{01,02}-\theta''_{01,02})\right]\end{aligned} \tag{4}$$

$$A_{x,y} = 2E_0^2J_0(\beta)J_1(\beta)\sqrt{r_{01,02}(\omega_0)} \tag{5}$$

$$\theta'_i = \varphi_m + \frac{\pi}{2} + \theta_i(\omega_0+\omega_m) - \theta_i(\omega_0) \tag{6}$$

$$\theta''_i = \varphi_m + \frac{\pi}{2} + \theta_i(\omega_0) - \theta_i(\omega_0-\omega_m) \tag{7}$$

Eq. (3) indicates that the proposed filter results from the combination of two filters determined by the shapes and phases of the two slightly separated notches along two principal axes given by the PM-PSFBG. The coherence between the two orthogonal filters is avoided in the optical domain, assuring a stable frequency response. It is noted that the effect induced by the time delay difference between the two filters on the performance-improved filter can be neglected thanks to small birefringence provided by the PM-PSFBG.

Numerical simulations are carried out using the above theoretical model. In the simulations, we select the effective refractive indices $n_{eff,01} = 1.45$, $n_{eff,02} = 1.450001$, and the refractive index modulation depths $\overline{\delta n_{eff,01}} = \overline{\delta n_{eff,02}} = 5.5\times10^{-4}$. Given that the Bragg wavelength of the fiber grating $\lambda_{01} = 1550$ nm is known, λ_{02} can be obtained from $\lambda_{02} = 2n_{eff,02}\Lambda$, Λ is the grating period. The total length of the PM-PSFBG is 8 mm. Two phase shifts are introduced along the fast and slow axes at the middle of the PM-PSFBG, and each phase shift is set at 1.05π. To obtain a smoothing reflection spectrum, the PM-PSFBG is apodized by a sinc function [22]. The simulated reflection spectra of the PM-PSFBG with a high resolution is presented in Fig. 2. As shown in Fig. 2, two ultra-narrow notches are clearly observed, and the two notches are located at about 1550.023 nm and 1550.024 nm, respectively.

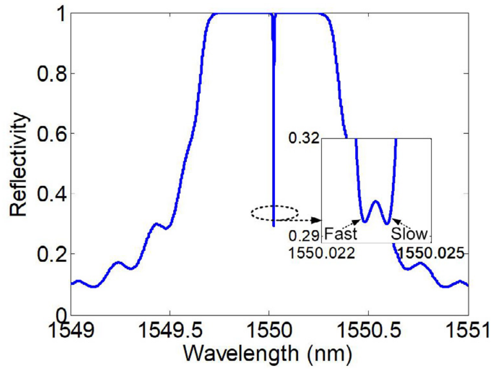

Fig. 2. Simulated reflection spectra of the PM-PSFBG.

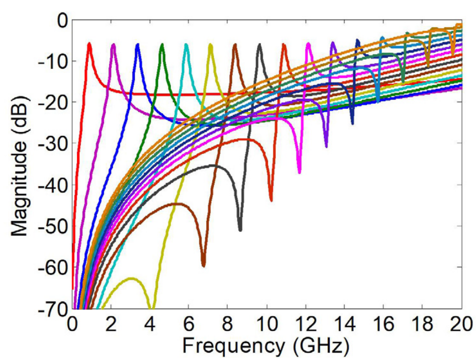

Fig. 3. Simulated conventional filter response with the center frequency tuning based on the conventional filter structure.

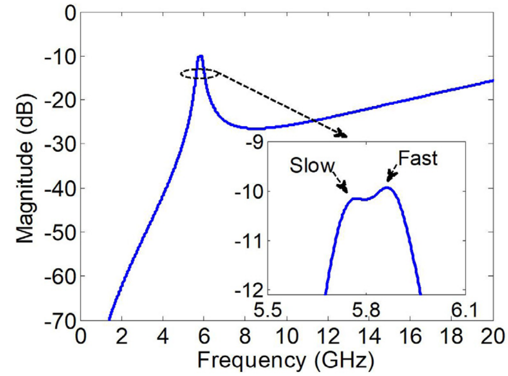

Fig. 4. Simulated filter response with two peaks induced by two notches along the fast and slow principal axes of the PM-PSFBG.

To investigate the improvement in out-of-rejection and frequency tuning range, three kinds of filter responses are theoretically analyzed. Firstly, the conventional single-passband filter based on a common PM and a common PSFBG is theoretically analyzed. Adjusting PC1 to make the polarization state of a light wave be aligned with one principal axis of the PolM, under this condition, the PolM is operating as a common PM for only one principle axis is utilized. Then the polarization state of the phase-modulated signal from the common PM is aligned with one principal axis of PM-PSFBG (e.g. fast axis) by adjusting PC2, in this case, the PM-PSFBG acts as a common PSFBG due to the use of only one principal axis. Thus, the conventional single-passband filter based on a common PM and a common PSFBG is constructed.

Fig. 3 plots the conventional filter response with the center frequency tuned by a frequency spacing of 1.25 GHz. As given by Fig. 3, with the center frequency tuned to high frequency, the out-of-band rejection ratio is first deteriorated gradually, and then the single-passband filter is switched to a single-notch filter when the frequency exceeds about 16 GHz because of the restricted reflection bandwidth of the equivalent common PSFBG.

Secondly, the polarization state of PC1 is held, and PC2 is adjusted to make the polarization state of the phase-modulated signal from the equivalent common PM be oriented 45° with respect to one principal axis of the PM-PSFBG. In this case, the modulated signal propagates along the fast and slow axes of the PM-PSFBG, and the corresponding filter response is presented in Fig. 4 with the wavelength of the LD set at 1550.07 nm. Two peaks with slight frequency interval are observed due to the small birefringence of the PM-PSFBG. The slight frequency interval is determined by the spectral interval between the two notches, which is dependent on the birefringence provided by the PM-PSFBG.

Finally, to evaluate the characteristic of the proposed filter, PC1 is adjusted to make the polarization state of the light wave to be oriented 45° with respect to one principal axis of the PolM, two phase-modulated signals with opposite modulation indices are generated. The two polarization states of the phase-modulated signals are subsequently aligned with, respectively, the fast and slow axes of the PM-PSFBG by means of PC2. After the two phase-modulated signals are reflected back from the PM-PSFBG, two conventional single-passband or two single-notch filters are achieved after photodetection. Since the two filters are out of phase, the subtraction between the two filters is performed. Therefore, a performance-improved filter is realized through subtraction. When the optical carrier shifts away small (large) from the notches, the performance-improved single-passband filter is resulted from subtraction of two conventional single-passband filters (two single-notch filters), as shown in Fig. 5 (Fig. 6). As can be seen, after subtraction, the out-of-band rejection of the performance-improved filter is more than twice of that of the conventional filter. It is worth noting that the notch filter previously operating in conventional filter is switched to a bandpass filter operating in the proposed single-passband filter. Therefore, the frequency tuning range of the proposed single-passband filter is significantly extended, compared to the conventional single-passband filter. To the best of our knowledge, it is first to utilize the subtraction of two single-notch filters to extend the frequency tuning range of a single-passband filter, overcoming the limitation of reflection bandwidth of the common PSFBG. When the wavelength of the LD is increased starting from 1550.03 nm, the center frequency of the performance-improved single-passband filter is shifted to high frequency with the passband bandwidth maintained, as plotted in Fig. 7. These plots show that the performance-improved single-passband filter is tunable over a frequency range from DC to 20 GHz, which clearly demonstrates that the frequency tuning range is significantly extended as compared to the conventional single-passband filter shown in Fig. 3.

3. Experimental results and discussion

A proof-of-concept experiment based on the configuration shown in Fig. 1 is set up. In the experiment, a light wave from a LD (Agilent N7714A) with its polarization state controlled by PC1 is sent to a PolM (Versawave Inc.) having a half-wave voltage of 3.5 V at 1 GHz, driven by a sweeping signal from a VNA (Rohde & Schwarz ZVA 67). The modulated light wave is amplified by an EDFA and subsequently sent into a PM-PSFBG via a circulator. The polarization states of the complimentary modulated signals are controlled by PC2. After reflection from the PM-PSFBG, the modulated signals are then launched into a PD (u^2t) with a responsivity of 0.65 A/W to recover the processed RF signal. Finally, the processed RF signal is analyzed by the VNA.

Fig. 8 shows the spectra of the reflection and transmission responses of the PM-PSFBG, and the inset displays the zoom-in view of the

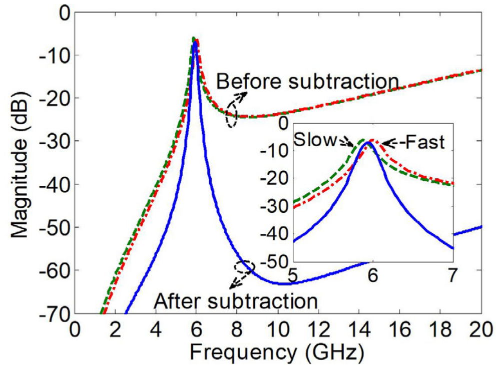

Fig. 5. Simulated performance-improved single-passband filter response resulting from subtraction of two single-passband filter responses.

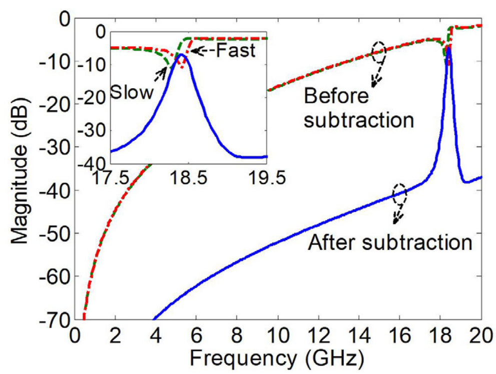

Fig. 6. Simulated performance-improved single-passband filter response resulting from subtraction of two single-notch filter responses.

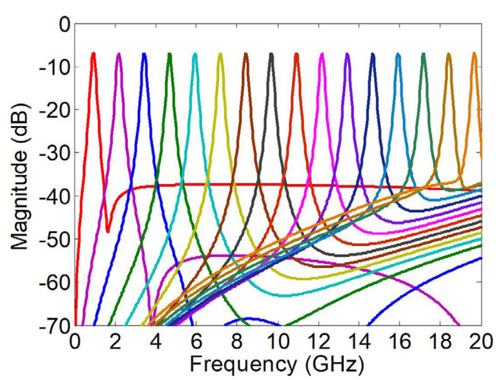

Fig. 7. Simulated performance-improved single-passband filter response with the center frequency tuning based on the proposed filter structure.

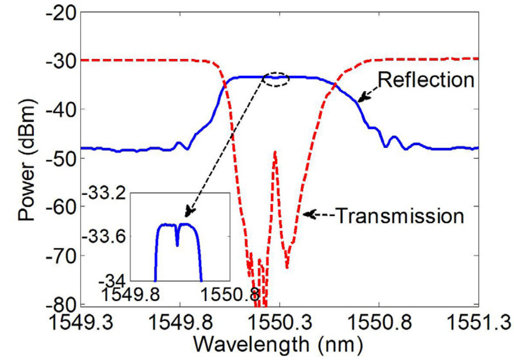

Fig. 8. Spectra of the reflection and transmission of the PM-PSFBG.

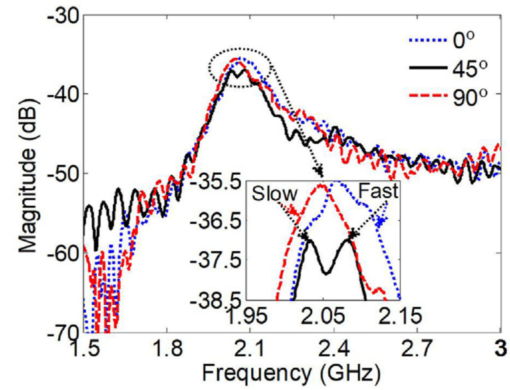

Fig. 9. Filter response with different polarization state of the phase-modulated signal relative to one principal axis of the PM-PSFBG.

notches. Since the birefringence of the PM-PSFBG is introduced during the manufacturing and the writing process of the PSFBG on a single-mode fiber [25], the birefringence is very small, leading to a very small spectral interval between the two notches. As a result, the two notches in reflection response or two passbands in transmission response cannot be differentiated from each other using the optical spectrum analyzer (OSA) with a limited resolution of 0.02 nm (2.5 GHz). The notches are located at around 1550.28 nm. As can be seen from the transmission response in Fig. 8, the position of the phase shift exhibits a small deviation from the middle of the transmission band as well as the middle of the reflection band.

To experimentally and extensively investigate the improvement in out-of-band rejection and frequency tuning range, we begin by demonstrating the birefringence property of the PSFBG. For this purpose, the polarization state of the light wave from the LD is aligned with one principal axis of the PolM, which serves as a common PM. Then the polarization state of the phase-modulated signal at the output of the equivalent common PM is oriented 45° with respect to one principal axis (e.g. fast axis) of the PM-PSFBG so that the two principal axes of the PM-PSFBG are activated. The resulting measured filter response is shown in Fig. 9, which exhibits two peaks corresponding to the two notches of the PM-PSFBG. For comparison, the frequency response with the polarization state of the phase-modulated signal oriented 0° or 90° relative to one principal axis of the PM-PSFBG is also shown in Fig. 9. It demonstrates that the PSFBG indeed has the birefringence property.

Next, we discuss the performance of the conventional single-passband filter. In doing so, the polarization state of the light wave aligned with one principal axis of the PolM is kept unchanged, but the polarization state of the phase-modulated signal is adjusted to be aligned with one principal axis of the PM-PSFBG by adjusting PC2. As the wavelength of the LD is increased from 1550.29 nm by a wavelength spacing of 0.02 nm, shifting away from the notches of the PM-PSFBG, a filter response with the center frequency tuned to high frequency by a frequency spacing of 2.5 GHz is obtained and shown in Fig. 10. From Fig. 10 one can see that the out-of-band rejection of the single-passband filter is very poor over a broad range from DC to 20 GHz, which is caused by the limiting notch rejection, bandwidth and slope of the PM-PSFBG, and the maximum out-of-band rejection ratio is only about 10 dB. Moreover, the single-passband filter is gradually converted to a single-notch filter, which exactly coincides with the preceding numerical simulation. The out-of-band rejection ratio of the single-passband filter is reduced gradually while the notch rejection ratio of the single-notch filter is increased with the center frequency shifted to high frequency. For the single-passband filter, the frequency tuning range is only about 8 GHz.

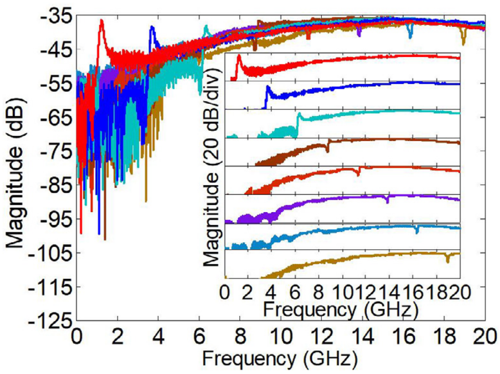

Fig. 10. Conventional filter response with the center frequency tuning based on the conventional structure.

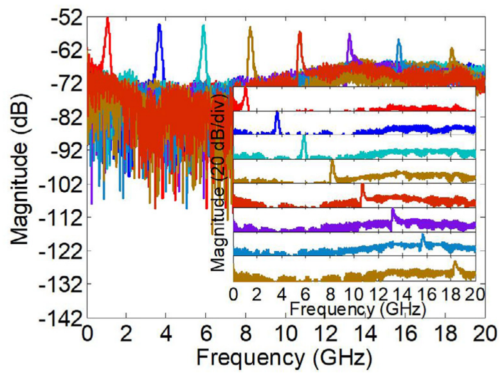

Fig. 11. Performance-improved single-passband filter response with the center frequency tuning based on the proposed structure.

Finally, we investigate the performance of the proposed filter in detail. In the proposed filter, PC1 is adjusted to ensure the polarization state of the LD is oriented 45° with respect to one principal axis of the PolM. At the output of the PolM, two phase-modulated signals with opposite indices are generated. The polarization states of the two phase-modulated signals are adjusted to be aligned with the fast and slow axes of the PM-PSFBG, respectively, by means of PC2. As the wavelength of the LD is increased from 1550.288 nm by a wavelength spacing of 0.02 nm, the proposed single-passband filter with the center frequency tuned by a frequency spacing of 2.5 GHz is achieved and depicted in Fig. 11. As shown in Fig. 11, the out-of-band rejection is improved greatly over a broad range from DC to 20 GHz because of subtraction of the two filters (two single-passband or two single-notch filters) with a slight frequency interval. The maximum out-of-band rejection ratio achieves up to about 18 dB, which is nearly twice of that of the conventional single-passband filter presented in Fig. 10. As expected, the single-notch filter previously operating in conventional structure shown in Fig. 10 is switched to a single-passband filter in the proposed filter shown in Fig. 11. The proposed single-passband filter can be clearly observed over a frequency range from DC to 20 GHz, which indicates that the frequency tuning range is significantly extended, as compared with the conventional filter. It is worth noting that, if the performance of the conventional single-passband filter is improved further by optimizing the PSFBG parameters [26], the performance of the proposed filter will be enhanced further by utilizing the birefringence of the PSFBG.

4. Conclusion

A proposed performance-improved single-passband filter was theoretically analyzed and experimentally demonstrated. By making the polarization state of the light wave be oriented 45° relative to one principal axis of a PolM, and thereby two phase-modulated signals with opposite phase modulation indices were generated. When the two polarization states of two phase-modulated signals were controlled to be aligned with the fast and slow axes of the PM-PSFBG with small birefringence, two single-passband or two single-notch filters with slight frequency interval were achieved. Since the two filters were out of phase, subtraction between the two filters was performed. Through subtraction, the out-of-band rejection was greatly improved, and the frequency tuning range was largely extended. Analytical simulations were carried out using the established theoretical model, which were finally demonstrated by experimental results. The experimental results indicated that the out-of-band rejection ratio was nearly doubled, and the extended frequency tuning range from DC to 20 GHz was achieved, compared to the conventional single-passband filter.

Acknowledgments

This work was supported by the Natural Science Foundation of China (No. 61302026, 61527820, 61275067) and the Scientific Research Foundation of Nanjing University of Posts and Telecommunications (No. NY218052).

References

[1] J. Capmany, D. Novak, Microwave photonics combines two worlds, Nat. Photonics 1 (2007) 319–330.
[2] J. Yao, Microwave photonics, J. Lightwave Technol. 27 (3) (2009) 314–335.
[3] J. Capmany, B. Ortega, D. Pastor, A tutorial on microwave photonic filters, J. Lightwave Technol. 24 (1) (2006) 201–229.
[4] R.A. Minasian, Narrow-passband and frequency-tunable microwave photonic filter based on phase-modulation to intensity-modulation conversion using a phase-shifted fiber Bragg grating, IEEE Trans. Microw. Theory Tech. 54 (2) (2006) 832–846.
[5] Y. Yan, S. Blais, J. Yao, Tunable photonic microwave bandpass filter with negative coefficients implemented using an optical phase modulator and chirped fiber Bragg gratings, J. Lightwave Technol. 25 (11) (2007) 3283–3288.
[6] N. You, R.A. Minasian, A novel high-Q optical microwave processor using hybrid delay-line filters, IEEE Trans. Microw. Theory Tech. 47 (7) (1999) 1304–1308.
[7] J. Mora, B. Ortega, A. Díez, J.L. Cruz, M.V. Andrés, J. Capmany, D. Pastor, Photonic microwave tunable single-bandpass filter based on a Mach–Zehnder interferometer, J. Lightwave Technol. 24 (7) (2006) 2500–2509.
[8] L. Li, X. Yi, T. Huang, R.A. Minasian, Shifted dispersion-induced radio-frequency fading in microwave photonic filters using a dual-input Mach–Zehnder electro-optic modulator, Opt. Lett. 38 (7) (2013) 1164–1166.
[9] T.H. Huang, X. Yi, R.A. Minasian, Single passband microwave photonic filter using continuous-time impulse response, Opt. Express 19 (7) (2011) 6231–6242.
[10] H. Wang, J. Zheng, W. Li, L. Wang, M. Li, L. Xie, N. Zhu, Widely tunable single-bandpass microwave photonic filter based on polarization processing of a nonsliced broadband optical source, Opt. Lett. 38 (22) (2013) 4857–4860.
[11] X. Xue, X. Zheng, H. Zhang, B. Zhou, Widely tunable single-bandpass microwave photonic filter employing a non-sliced broadband optical source, Opt. Express 19 (19) (2011) 18423–18429.
[12] X. Xue, X. Zheng, H. Zhang, B. Zhou, All-optical microwave bandpass filter and phase shifter using a broadband optical source and an optical phase modulator, Opt. Lett. 37 (10) (2012) 1661–1663.
[13] R. Tao, X. Feng, Y. Cao, Z. Li, B. Guan, Widely tunable single bandpass microwave photonic filter based on phase modulation and stimulated Brillouin scattering, IEEE Photonics Technol. Lett. 24 (13) (2012) 1097–1099.
[14] W. Zhang, R.A. Minasian, Widely tunable single-passband microwave photonic filter based on stimulated Brillouin scattering, IEEE Photonics Technol. Lett. 23 (23) (2011) 1775–1777.
[15] Y. Yu, J. Dong, E. Xu, X. Li, L. Zhou, F. Wang, X. Zhang, Single passband microwave photonic filter with continuous wideband tunability based on electro-optic phase modulator and Fabry–Pérot semiconductor optical amplifier, J. Lightwave Technol. 29 (23) (2011) 3542–3550.
[16] Y. Deng, M. Li, J. Tang, S. Sun, N. Huang, N. Zhu, Widely tunable single-passband microwave photonic filter based on DFB-SOA-assisted optical carrier recovery, IEEE Photonics J. 7 (5) (2015) 5501108.
[17] E. Xu, Z. Zhang, P. Li, Tunable single-passband microwave photonic filter based on Sagnac loop and Fabry–Perot laser diode, Chin. Phys. Lett. 34 (1) (2017) 014203.
[18] F. Jiang, Y. Yu, H. Tang, L. Xu, X. Zhang, Tunable bandpass microwave photonic filter with ultrahigh stopband attenuation and skirt selectivity, Opt. Express 24 (16) (2016) 18655–18663.
[19] E. Xu, J. Yao, Frequency- and notch-depth-tunable single-notch microwave photonic filter, IEEE Photonics Technol. Lett. 27 (19) (2015) 2063–2066.

[20] W. Li, M. Li, J. Yao, Narrow-passband and frequency-tunable microwave photonic filter based on phase-modulation to intensity-modulation conversion using a phase-shifted fiber Bragg grating, IEEE Trans. Microw. Theory Tech. 60 (5) (2012) 1287–1296.
[21] X. Han, E. Xu, W. Liu, J. Yao, Tunable single bandpass microwave photonic filter with an improved dynamic range, IEEE Photonics Technol. Lett. 28 (1) (2016) 11–14.
[22] E. Xu, Z. Zhang, P. Li, Highly flexible microwave photonic single-passband filter, IEEE Photonics J. 9 (1) (2017) 5500213.
[23] Y. Wang, M. Wang, W. Xia, X. Ni, D. Wu, Optical fiber Bragg grating pressure sensor based on dual-frequency optoelectronic oscillator, IEEE Photonics Technol. Lett. 29 (21) (2017) 1864–1867.
[24] T. Erdogan, Fiber grating spectra, J. Lightwave Technol. 15 (8) (1997) 1277–1294.
[25] R. Gafsi, M.A. El-Sherif, Analysis of induced-birefringence effects on fiber Bragg gratings, Opt. Fiber Technol. 6 (2000) 299–323.
[26] H.S. Daniel, G.K. Gopalakrishnan, Extended DC-20.0 GHz tunable photonic microwave filter with high out-of-band rejection, Electron. Lett. 53 (9) (2017) 613–614.